

# Cell type specific firing patterns in a V1 cortical column model depend on feedforward and feedback activity

Giulia Moreni<sup>1,2,\*</sup>, Cyriel M. A. Pennartz<sup>1,2</sup> and Jorge F. Mejias<sup>1,2,\*</sup>

<sup>1</sup>Cognitive and Systems Neuroscience Group, Swammerdam Institute for Life Sciences, Faculty of Science, University of Amsterdam, 1090 GE Amsterdam, the Netherlands

<sup>2</sup>Research Priority Area Amsterdam Brain and Cognition, University of Amsterdam

\*Corresponding author: Giulia Moreni ([g.moreni@uva.nl](mailto:g.moreni@uva.nl)), Jorge F. Mejias ([j.f.mejias@uva.nl](mailto:j.f.mejias@uva.nl))

## Abstract

Stimulation of specific cell groups under different network regimes (e.g., spontaneous activity or sensory-evoked activity) can provide insights into the neural dynamics of cortical columns. While these protocols are challenging to perform experimentally, modelling can serve as a powerful tool for such explorations. Using detailed electrophysiological and anatomical data from mouse V1, we modeled a spiking network model of the cortical column microcircuit. This model incorporates pyramidal cells and three distinct interneuron types (PV, SST, and VIP cells, specified per lamina), as well as the dynamic and voltage-dependent properties of AMPA, GABA, and NMDA receptors. We first demonstrate that thalamocortical feedforward (FF) and feedback (FB) stimuli arriving in the column have opposite effects, leading to net columnar excitation and inhibition respectively and revealing translaminar gain control via full-column inhibition by layer 6. We then perturb one cell group (defined by a cell type in a specific layer) at a time and observe the effects on other cell groups under distinct network states: spontaneous, feedforward-driven, feedback-driven, and a combination of feedforward and feedback. Our findings reveal that when the same group is perturbed, the columnar response

may vary significantly based on its state, with strong sensory feedforward input decreasing columnar sensitivity to all perturbations and feedback input serving as modulator of intra columnar interactions. Given that activity changes within specific neuronal populations are difficult to predict a priori and considering the practical challenges of conducting experiments, our computational simulations can serve as a critical tool to predict outcomes of perturbations and assist in the design of future experimental planning.

## Introduction

The intricate architecture of the cerebral cortex, with its diverse neuronal populations and complex connectivity patterns, plays a pivotal role in processing sensory information and orchestrating cognitive functions<sup>1,2</sup>. Central to this architecture is the column-like circuitry, a functional unit that has been the subject of extensive research over the years<sup>3,4,5</sup>. Within these columns, different neuronal populations interact in a dynamic manner<sup>6</sup>, giving rise to a rich repertoire of activity patterns that can be modulated by both internal and external factors<sup>7</sup>. One of the intriguing aspects of cortical columns is the interplay between excitatory and inhibitory neuronal populations. This balance, often referred to as E/I balance, is crucial for maintaining stable network dynamics and ensuring efficient information processing.<sup>8–13</sup>. Disruptions in this balance can lead to various neurological and psychiatric disorders (such as schizophrenia and autism) underscoring its importance<sup>14,15</sup>. In recent years, there has been a growing interest in understanding how different types of input, such as cortical and thalamic feedforward (FF) and feedback (FB) signals, modulate the activity within cortical columns<sup>16–19</sup>. These inputs can have profound effects on the firing rates of different neuronal populations, leading to diverse patterns of network activity<sup>17,18</sup>. However, the precise mechanisms through which these inputs shape cortical dynamics remain a topic of active investigation<sup>20</sup>.

In this study, we delve into the behaviour of a cortical column model under different conditions. We explore how spontaneous activity, feedforward input and feedback input influence the activity of different neuronal populations within the cortical column. This was done using a biologically detailed computational model of a cortical column of mouse primary

visual cortex V1<sup>21</sup>. This model incorporates dynamic properties of multiple postsynaptic receptors (AMPA, NMDA, and GABA-A receptors), and is tightly constrained by state-of-the-art cortical connectivity data on mouse V1<sup>22-23</sup> which include cell densities and laminar-specific connectivity patterns across four different cell types (pyramidal neurons and PV, SST and VIP interneurons) and five laminar modules (layers 1, 2/3, 4, 5 and 6). Our simulations show that feedforward and feedback stimuli have opposing impacts on columnar activity, leading to net columnar excitation and inhibition, respectively, in agreement with experimental and other modelling work<sup>17,24-26</sup>. Furthermore, our model reveals a translaminar inhibitory effect mediated by layer 6 activity, in line with a role in columnar gain control role as suggested by experiments<sup>27,28</sup>. However, our model reveals that such inhibition may well be the consequence of complex cortical interactions and not only of the recruitment of local inhibitory cells as previously suggested. We then stimulated one cell group at a time in distinct states (spontaneous, sensory feedforward-driven, feedback-driven, and a state driven by a combination of feedforward and feedback stimuli) and observed the effects on the other populations. These pertubational experiments reveal multiple group-to-group dependencies which vary across the different states considered, with strong feedforward input decreasing overall columnar sensitivity and feedback input modulating interactions linked lateral, inter-columnar communication. In addition, our findings proved the distinctive roles of inhibitory neurons in network dynamics. For instance, our model predicts that in an experimental setting with strong top-down modulation of V1—such as input to excitatory neurons in layer 5—providing stimuli to different inhibitory neurons in layer 6 will induce contrasting responses in the E2/3 neurons, depending on the specific inhibitory subgroup targeted. This model illuminate the complex interplay between different types of inputs and their impact on cortical dynamics and it can be used as a predictive tool to guide and design experiments. Moreover, our results reveal that when the same group is stimulated, the network's response can vary significantly based on its initial state.

## Results

We begin by describing our cortical column model, sketched in Fig. 1A. We consider a network of 5,000 spiking neurons which are distributed across five laminar modules, four of which (layers 2/3, 4, 5 and 6) contain pyramidal neurons as well as PV, SST and VIP cells, and one of which (layer 1) contains only VIP cells. For laminar modules with multiple cell types, about 85% of the cells are pyramidal neurons and the remaining 15% are inhibitory interneurons –with the precise proportion of each inhibitory cell type in each layer given by anatomical data<sup>23</sup> and depicted in Fig. 1A as the relative size of the respective inhibitory population (see Moreni et al.<sup>9</sup>).

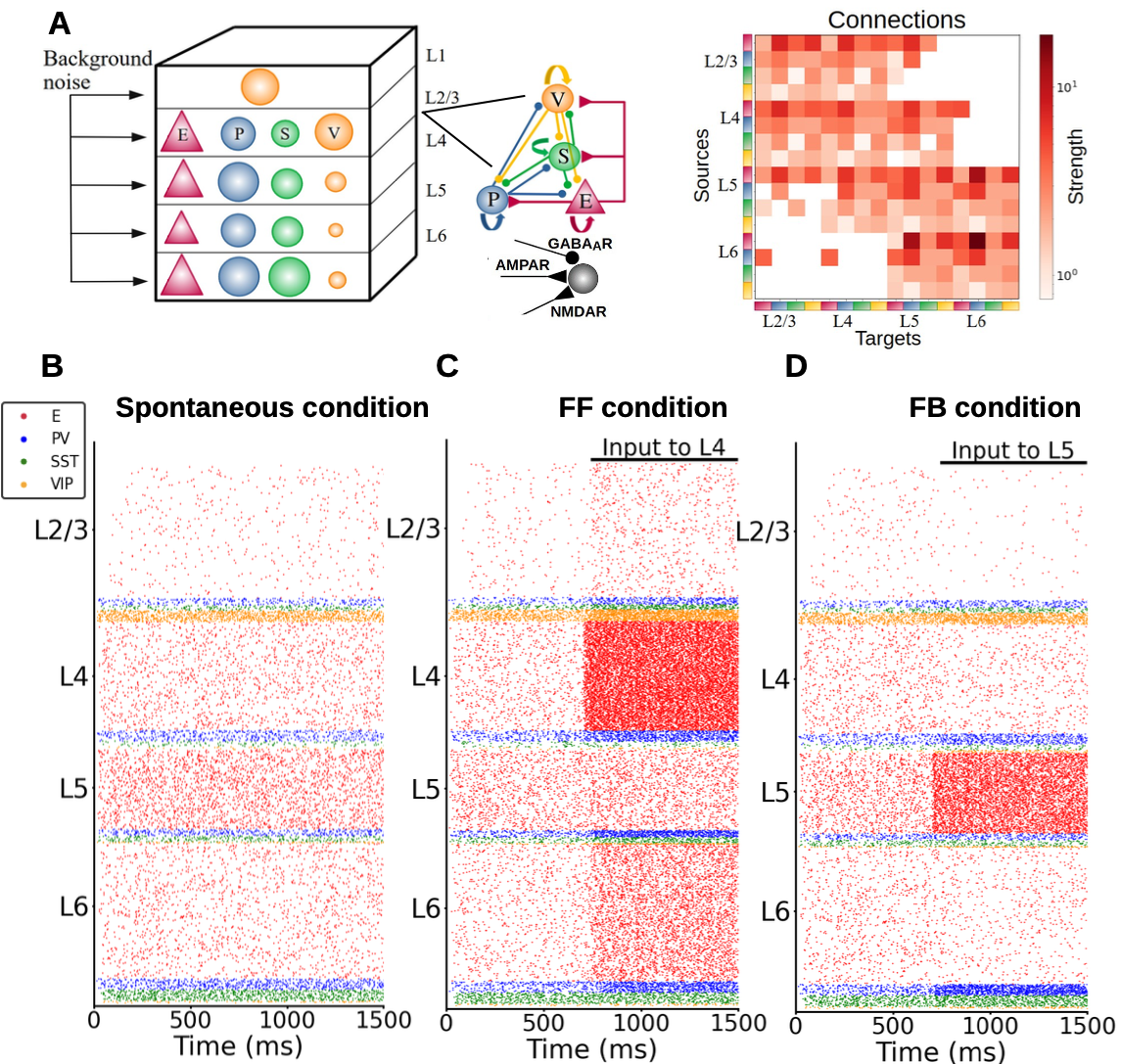


*Figure 1: (A) Sketch of the cortical column model. In layers 2/3, 4, 5, and 6 an excitatory population E (red triangles) and 3 types of inhibitory population (PV, SST, VIP cells as blue, green, orange circles: P, S and V, respectively) are present. In layer 1 only VIP cells are present. The size of the circles in the top-left panel represents the relative size of the inhibitory populations. Connections*

*between groups are not shown in the top left diagram; the zoomed-in schematic to the right shows inter-population connectivity and postsynaptic receptors (AMPA, GABA<sub>A</sub>, NMDA) involved. The connectivity matrix is shown at the right. (B)-(D) Network in three different states. (B) Spontaneous (resting) condition. Simulated firing rates match experimental firing rates<sup>21</sup>. (C) Feedforward-driven condition (i.e., with excitatory input to L4 pyramidal cells). At 700ms an constant input of 30 pA is injected to all L4 pyramidal cells and excitatory neurons in all layers increase their activity. (D) One feedback-driven condition (i.e., with excitatory 30 pA input to L5 pyramidal cells). At 700ms an input is injected in L5, and excitatory neurons in all other layers decrease their activity while interneurons in layer 6 increase their firing.*

### **Three distinct states: spontaneous, feedforward-driven and feedback-driven**

We begin by considering three states of the system: spontaneous, feedforward-driven and feedback-driven. In the spontaneous condition (Fig. 1B), the column receives only background input to all cells (Table S9), needed to match the cell-type-specific firing rates observed *in vivo* in mice<sup>21</sup>. When subjected to feedforward input evoking the arrival of bottom-up sensory stimuli (i.e., input to all pyramidal neurons in layer 4), the system displays an increase in neuronal activity in all cell types across all other layers (Fig. 1C). These stimulus-triggered firing rate responses are in line with experimental observations *in vivo*<sup>21</sup>. On the other hand, feedback signals corresponding to top-down modulations from higher cortical areas can be simulated by injecting external current into layer 5 pyramidal neurons<sup>17,19,29,30</sup>. Our findings indicate that while feedback input augments the activity of layer 5 pyramidal neurons, it concurrently reduces the firing rates of all other pyramidal neurons in the column, resulting in an overall inhibition of pyramidal cells (Fig. 1D). This phenomenon can be attributed to the modulation of inhibitory neurons, particularly in L4 and L6, which, due to feedback input, significantly increase their activity, inhibiting the pyramidal cells. Consequently, the impact of feedback input stands in contrast to what is observed with feedforward input.

### **Perturbations of specific cell types in spontaneous and feedforward-driven states**

Next, we systematically tested the response of the columnar model to perturbational excitatory inputs to every cell type and layer in the column, for both the spontaneous (Fig. 1B) and stimulus-evoked (Fig. 1C) conditions. Perturbative input targeted to specific cell types allowed us to explore the role of each layer- and type-specific cell in the overall columnar dynamics, as

previously done for simpler neural circuits<sup>31</sup>. This will allow us to understand whether the responses to perturbations are dependent on the initial state of the cortical column. To quantify the effects of input perturbations in our network, we defined the response matrix as an array  $R_{XY}$  describing the activity change of population X as a result of the perturbative input to population Y. Fig. 2 shows response matrices for spontaneous and feedforward-driven conditions (Fig. 2A and 2B) and their differences (Fig. 2C). We first put the network in a 'state', for example spontaneous condition or feedforward condition (i.e. input to layer 4 pyramidal cells) and then we inject input to one cell group at a time; we then observe the effects on the other neuron groups to build the matrix. Details on how the matrix is computed are provided in the Methods section. We will refer to this process of perturbing one cell group at a time and observing the effect on the others as 'perturbation analysis'. Overall, effects on any given population are difficult to predict a priori, highlighting the importance of computational tests to guide intuition<sup>31,32</sup>. For example, when we perturbed layer 2/3 pyramidal neurons in the spontaneous state, we observed a substantial increase in layer 5 PV activity (Fig. 2A), even though according to the connectivity data and canonical microcircuit principles<sup>1,23</sup>, the strongest anatomical projection from layer 2/3 to layer 5 was between their pyramidal neurons. The results also change depending on the condition: as Fig. 2 shows, a small perturbative input to pyramidal neurons in layer 2/3 increases the firing rate of PV cells in layer 5 in spontaneous conditions, but the same stimulus induces only minor changes in PV activity during the stimulus-evoked condition (compare rate plots in 2A and 2B). Other features remain invariant across conditions: perturbing layer 6 pyramidal neurons acts as a suppressor of superficial layers (2/3 and 4) and activator of deep layers (5 and 6) in both conditions. This aligns with experimental observations which characterize layer 6 as a translaminar inhibitor<sup>28</sup>; our model reveals that such inhibition may well be the consequence of complex cortical interactions and not only of the recruitment of local inhibitory cells. The model might help us explain the dynamics causing the increase in activity within layer 5. By observing the connectivity matrix (Fig. 1A), we note that pyramidal cells in layer 6 are strongly connected to PV cells in layer 5, making it intuitive to expect an increase in the activity of PV cells in layer 5 when layer 6 pyramidal cells are perturbed. This, in turn, might be one of the factors responsible for the

decrease in activity of pyramidal cells in layer 5. A case-by-case comparison between the effects in spontaneous and feedforward-driven conditions (Fig. 2C) reveals a wide variability of effects across the matrix. For example, our model predicts a difference in the response of SST cells in layer 4 when perturbing pyramidal cells in layer 4 in two scenarios. In the spontaneous case, the SST cells increase their activity, whereas in the feedforward case, no significant change is induced. We can speculate that feedforward input has a stabilizing effect in the context of perturbation. In fact, when comparing the two conditions (Fig. 2C), we note that most perturbations become non-significant in the feedforward case.

Other differences between the two scenarios supporting this idea are the following:

- 1) In the spontaneous case, pyramidal cells in layer 4 show rate changes induced by the perturbation of several interneurons in several layers (VIP 2/3, PV 4, VIP 4, SST 5, PV 6). In the feedforward case, these changes are irrelevant (<20%), see Fig. 2C.
- 2) In the spontaneous case, perturbation of SST cells in layer 5 shows a significant negative rate change in many cells in non-superficial layers (E 4, PV 5, VIP 5, E 6); this is not observed in the feedforward condition (Fig. 2C).
- 3) In the spontaneous case, perturbation of pyramidal cells in layer 5 induces a significant positive rate change in several cell types (SST 2/3, VIP 2/3, SST 4), which is irrelevant in the feedforward condition (Fig. 2C).

This observation shows that in the feedforward case, the model is more robust against small perturbations. Moreover, our model can act as a prediction for experiments. This analysis indicates, as also shown by previous studies<sup>31</sup>, that simple intuition sometimes leads to wrong conclusions, or overgeneralization, in models of cortical circuits with multiple cell types.

We next performed an extensive perturbation analysis for 15 different scenarios. In each scenario, we varied the strength of (non-perturbational) feedforward input injected into excitatory neurons in layer 4, mimicking activation by retino-thalamic input. The input strength ranged from 0 to 80 pA. For each condition, we generated a perturbation matrix by giving input

to one neuronal group at a time and observed the changes in the others (as above). We then counted the number of marked changes (more than a 20% increase or decrease) in their firing rates upon the injection of perturbational input into any population. We observed that networks with stronger feedforward input display less marked changes upon perturbations than networks with weak feedforward input (Fig. 2D). The condition maximizing the number of changes was being in a state of receiving weak ( $\sim 10$  pA) feedforward input, indicating that input perturbations (presumably coming from other cortical circuits) have a stronger influence on visual cortex when animals receive weak visual input.

This result might seem in contrast with our common intuition: Feedforward (FF) input would generally increase the firing rates of neurons across the network. As a result of increased firing rates, the intuitive expectation is that any perturbations (especially to inhibitory neurons) would likely have a more pronounced effect in reducing the overall firing rates because there's more activity to suppress. However, contrary to these hypotheses, we observe that the network becomes more resilient to perturbations. We may explain this phenomenon by noting that when feedforward (FF) input is strong, the overall cellular activity reaches such a high level that minor perturbations are insufficient to alter the collective outcome.

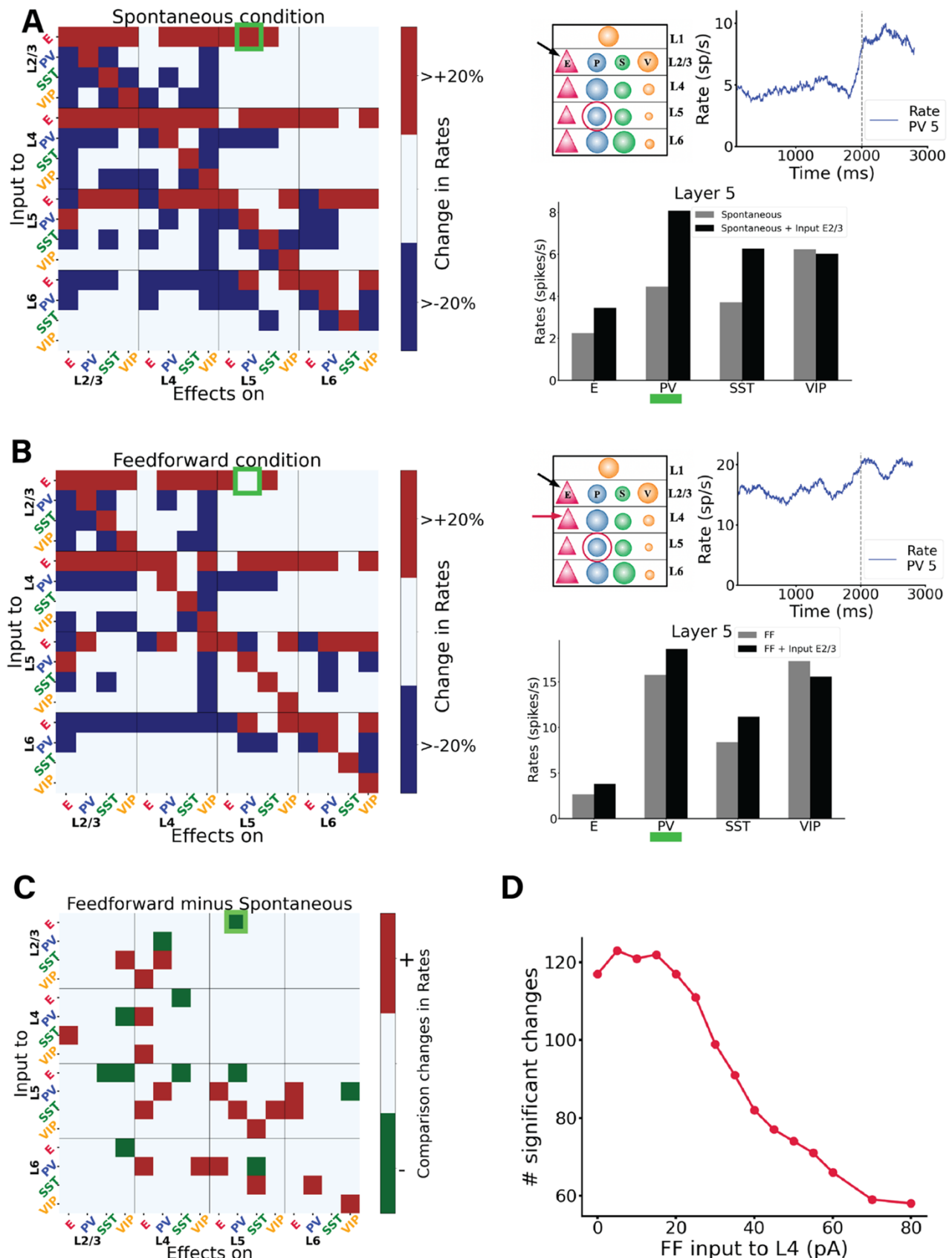


Figure 2. Perturbations of specific cell types in spontaneous and feedforward-driven states. (A) Matrix of input-output

*relationships of the network in the spontaneous state. We delivered excitatory input to one population (Y-axis; see Methods) and observed its effect on others (X-axis), repeating this for all 16 populations to construct the matrix. Red signifies an increase in mean firing rate by more than 20% above baseline, blue indicates a decrease by more than 20%, and white denotes changes less than 20%. We stimulated each subpopulation with a 30 pA DC current and monitored the resultant firing rate changes in all other subpopulations. The right panel of (A) details one specific simulation, where input to the E2/3 population is applied, and the impact on PV cells in layer 5 is measured. The dashed line corresponds to the stimuli onset, the blue trace represents firing rate, while the box plot compares firing rates before and after input injection to E2/3. Here, the PV interneurons in layer 5 respond more robustly than in the feedforward condition depicted below. (B) Displays the response matrix for the feedforward-driven state, wherein excitatory input is provided to L4 pyramidal cells. The right panel presents the same example as in (A) under this condition. (C) Matrix illustrating the difference between the two conditions, where white indicates no change, red a positive difference (i.e., a firing rate increase in the FF condition as compared to spontaneous condition), and green a negative difference (see Methods for detailed specifications). Comparing the two shows that overall in the feedforward case many firing rate changes becomes irrelevant (<20%) compared to the spontaneous case. (D) shows the number of significant changes in the corresponding perturbation matrix. We conducted perturbation analysis for 15 different network conditions, defined by varying Feedforward (FF) input to layer 4, and resulting in a 16x16 matrix for each condition, though these matrices are not displayed here. Each condition varied the input strength to excitatory neurons in layer 4 (E4), values on the X-axis range from 0 to 80 pA. The Y-axis represents the number of significant alterations in the respective matrix (the sum of red and blue squares). Increased input to layer 4 results in fewer perturbation-induced changes in the firing rates of other populations.*

## Perturbations in the feedback-driven state

We subsequently examined the model's response to perturbative excitatory inputs to each cell type and layer in the feedback-driven state, i.e. in a cortical column receiving feedback drive in layer 5 pyramidal cells (Fig. 1C). The corresponding response matrix<sup>31</sup> and its comparison with the spontaneous case are depicted in Fig. 3 (A and B panels respectively), which shows that a majority of perturbations results in positive changes, indicated by the prevalence of red over green squares. This can be explained from the fact that it is easier to excite a network that is already inhibited, in this case by feedback to layer 5. Consequently, in the presence of feedback, perturbations from adjacent circuits (like neighbouring cortical columns) become effectively excitatory overall. This indicates that feedback input to cortical columns may serve as a control mechanism to modulate lateral interactions across V1 columns, as also suggested by experimental findings<sup>33,34</sup>.

We next performed an extensive perturbation analysis for 15 different scenarios, similarly to what was previously done for the feedforward case. In each scenario, we varied the strength of

(non-perturbational) feedback input injected into excitatory neurons in layer 5. The input strength ranged from 0 to 80 pA. For each condition, we generated a perturbation matrix by giving input to one neuronal group at a time and observed the changes in the others. We then counted the number of marked changes (more than a 20% increase or decrease) in their firing rates upon the injection of perturbational input into any population. We observed that networks with stronger feedback input display fewer marked changes upon perturbations than networks with weak feedback input (Fig. 3C). In Supplementary Fig. S2, we also provide, among the marked changes, the percentage of positive changes (being roughly half of all of them) for each scenario. This result is similar to the one previously obtained by varying feedforward input strength. Probably the reason behind this is that when we have a strong feedback input which is governing the overall behaviour small perturbative inputs have irrelevant effect.

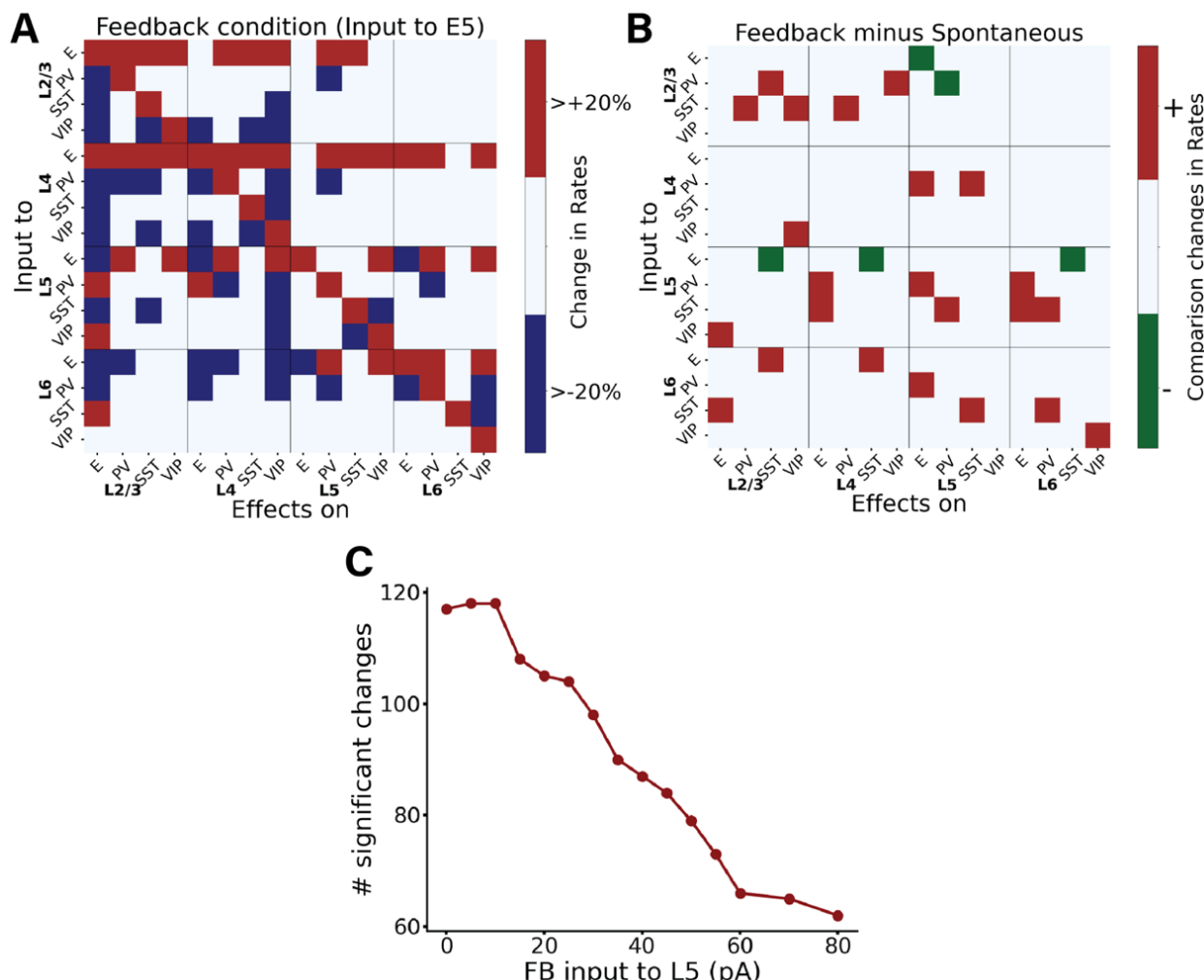


*Figure 3: Perturbational input-output matrix in feedback-driven condition. (A) Perturbational matrix of input-output relationships within the network. With feedback input (input to pyramidal cells in layer 5) applied, we administered input to one population (indicated on the Y-axis) and observed the effects on the others (X-axis). This process was repeated for all 16 populations to compile the matrix. Red signifies an increase in the mean firing rate exceeding 20% above the initial value (with only input to E5), blue denotes a decrease greater than 20%, and white represents a change less than 20%. (B) Comparative matrix between the feedback and spontaneous conditions (layout as in Fig. 2B). (C) shows the number of significant changes in the corresponding perturbation matrix. We conducted perturbation analysis for 15 different network conditions, defined by varying Feedback (FB) input to layer 5, and resulting in a 16x16 matrix for each condition, though these matrices are not displayed here. Each condition varied the input strength to excitatory neurons in layer 5, values on the X-axis range from 0 to 80 pA. The Y-axis represents the number of significant alterations in the respective matrix (the sum of red and blue squares). Increased input to layer 5 results in fewer perturbation-induced changes in the firing rates of other populations.*

Contrary to the more stereotypical feedforward input from sensory streams, which commonly targets excitatory neurons in layer 4, feedback projections have more diverse cellular targets<sup>35</sup> and synaptic projections may target several layers, with the notable exception of layer 4 which is consistently avoided by feedback projections<sup>19,36</sup>. This makes evaluating the effect of feedback modulation computationally more difficult. Therefore, in addition to the previously analysed feedback condition (input to only pyramidal neurons in layer 5), we explored four alternative feedback configurations (Fig. 4A), in which input respectively arrived at: (i) layer 2/3 pyramidal cells, (ii) pyramidal cells in layers 2/3 and 5, (iii) pyramidal and PV cells in layer 5, and (iv) pyramidal cells in layer 6. The evoked laminar spiking activity for each of these four alternative configurations (with feedback input arriving at 700 ms) is displayed in Fig. 4 panels A1-4, and we observed overall excitation for case A1 (especially in L2/3 and L5), slight inhibition in case A2 (leaving aside L5 and L2/3 pyramidal cells), no big effects in A3 (leaving aside L5), and overall inhibition in case A4 (leaving aside L6 cells), again in agreement with the translaminar inhibitory effect of layer 6 observed experimentally<sup>28</sup>.

The respective perturbational input-output matrices for configurations A1-4 are shown in Fig. 4B (subpanels B1-B4), and reveal that perturbational effects are overall similar for all four feedback configurations, with the number of significant changes being approximately equal for all configurations (Suppl. Fig. S1). This suggests that, from a global point of view, responses to perturbational input (such as lateral interactions) will be relatively insensitive to the type of

feedback pathway present, as long as the column is in a feedback-driven state. This robustness of feedback modulation effects should, however, be contrasted with several notable exceptions. For example, perturbations to SST and VIP cells in layer 6 alone never triggered a significant response in pyramidal cells of other layers, except for the last configuration (B4, feedback targeting pyramidal layer 6). In this scenario, pyramidal cells in layer 2/3 increase their activity when perturbation is applied to layer 6 SST or VIP cells, and decrease it when it is applied to layer 6 PV cells –highlighting cell-type selective modulation across layers. Different perturbation effects are observed in layer 2/3 SST and VIP populations when layer 5 pyramidal cells are stimulated, varying across configurations B1-2 and B3-4. Specifically, SST and VIP activities increase in configurations B1-2, whereas their firing rates do not change significantly in B3-4.

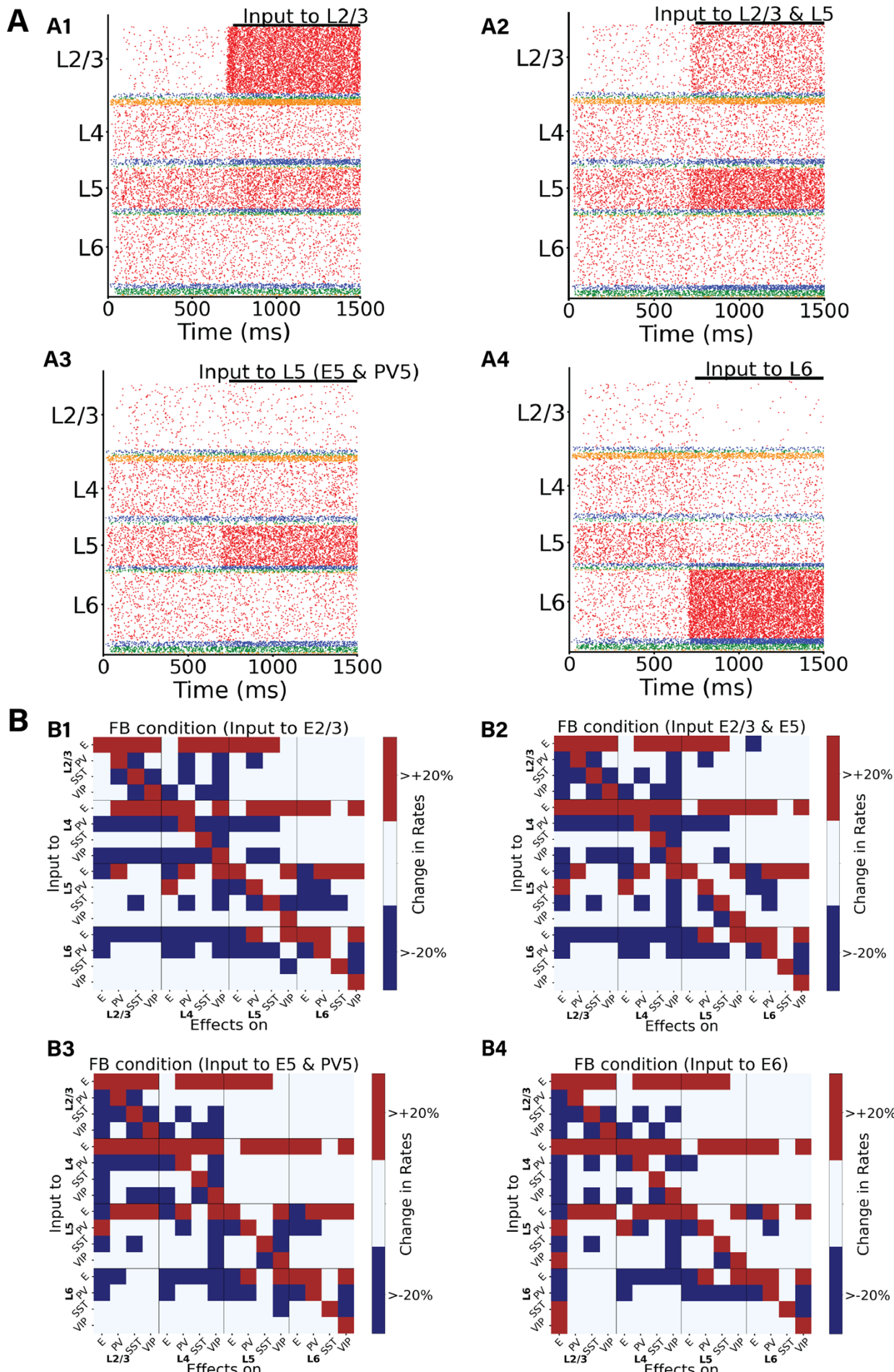


*Figure 4: Perturbation analysis in four different feedback-driven states. (A) Raster plots depicting four different states. The network state after 700 ms in the raster plot indicates the condition for the subsequent perturbation analysis. (B) Perturbation Input-output matrices for four distinct states: B1) Feedback input to excitatory neurons in layer 2/3. B2) Input to excitatory neurons in layer 2/3 and layer 5. B3) Input to both PV neurons and excitatory neurons in layer 5. B4) Input to excitatory neurons in layer 6. Within each condition, we delivered input to one population (Y-axis) and observed the resultant effects on the others (X-axis). We replicated this procedure for all 16 populations to derive each matrix. For color code, see Fig. 2.*

### **Integration of feedforward and feedback signals in the column**

Under realistic conditions, cortical columns in V1 may operate in a mixed regime, in which the column receives both sensory feedforward and modulatory feedback signals simultaneously. To explore this case, we analysed the impact of feedback modulation (i.e., input to layer 5) on a stimulus-evoked response that had been introduced shortly before (input to layer 4). The two inputs exhibited opposing effects: while feedforward input to layer 4 (introduced at 500 ms) augmented the activity of other pyramidal cells in all other layers, feedback input (introduced at 1100 ms) reduced it (Fig. 5A). In the isolated feedback scenario (Fig. 1C), we established that feedback input led to a decrease in the firing rates of all other pyramidal neurons than those in layer 5, resulting in a comprehensive inhibition of the circuit. Consequently, when both feedforward and feedback inputs were introduced at different intervals, their antagonistic roles became evident. For example, in layer 2/3 (and to some extent in layer 6), the feedback input adjusted the excitatory firing rates to levels similar to those observed prior to the introduction of feedforward input, effectively neutralizing the impact of the latter (Fig. 5A). To be more specific, upon arrival of feedback input to layer 5 pyramidal cells at 1100 ms, there was a discernible decrease in the activity of pyramidal cells across all layers, naturally with the exception of layer 5. This change can be attributed to inhibitory neurons, especially those in layers 4 and 6. Due to feedback input to layer 5 pyramidal cells projecting to these neurons, they significantly increased their activity across all layers, thereby inhibiting the pyramidal cells in L2/3, L4 and L6.

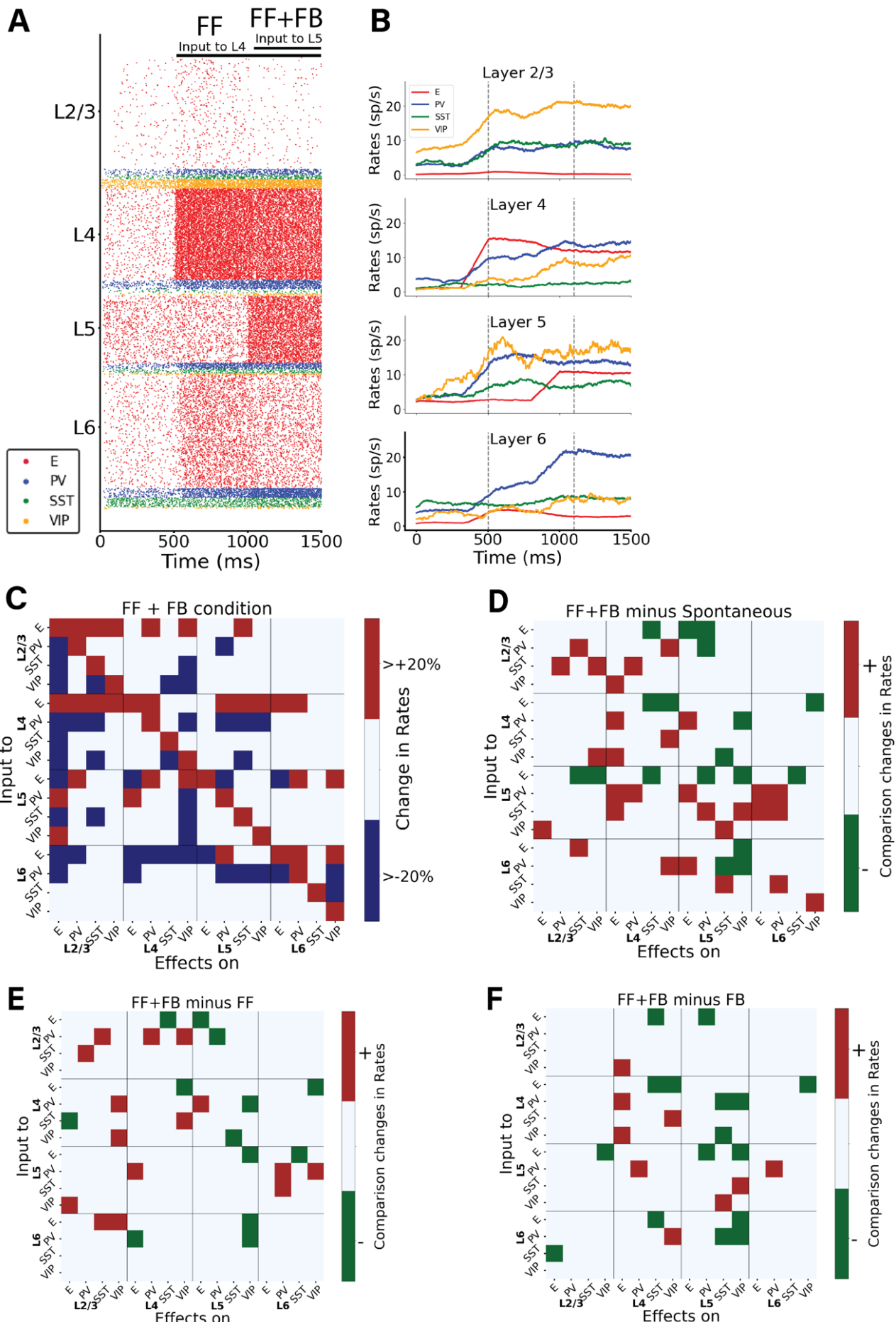


*Figure 5: Interaction between bottom-up and top-down signals in the cortical column model. (A) Raster plot of network activity with bottom-up and top-down input. At 500 ms a prolonged (feedforward) input is applied to layer 4 excitatory neurons (E4) and at 1100 ms an input is applied to layer 5 excitatory neurons (E5). The input to E5 has a largely opposite effect compared to the input to E4: it decreases the activity of excitatory neurons in layers 2/3, 4 and 6. (B) Mean firing rate traces of the various populations in each layer. Vertical dashed lines: onset of FF at 500 ms; onset of FB at 1100 ms. (C) Matrix of input-output relationships of the network. When both inputs to E4 and E5 are present, we delivered an input to one population (plotted on the Y-axis) and observed the effect on the others (X-axis). We repeated this procedure for the 16 populations to obtain the matrix. Color code as in Fig 2. (D) Matrix showing the difference between the feedback & feedforward situation and the spontaneous condition. (E) Matrix showing the difference between the feedback & feedforward situation and the feedforward only condition. (F) Matrix showing the difference between the feedback & feedforward situation and the feedback only condition.*

We subsequently conducted a systematic examination of the model's response to perturbative excitatory inputs directed at each cell type and layer within the column, specifically under conditions where both feedforward and feedback inputs were active (Fig. 5). The response matrix for the columnar model reveals intricate reactions to cell-type specific inputs. For instance, there is a pronounced inter-laminar inhibition affecting most cell types in layers 2/3 and 4 when pyramidal neurons in layer 6 are excited, reflecting again the role of layer 6 as translaminar inhibitor reported experimentally<sup>28,29</sup>. Conversely, inputs to pyramidal neurons in layers 2/3 and 4 induce widespread excitation in almost all cells within those layers. Lastly, stimulating interneurons results in a combination of effects. In Figure 5, panels D, E, and F offer a direct comparison of the response matrices from the spontaneous state (Fig. 2A), the feedforward-driven state (Fig. 2B), and the feedback-driven state (Fig. 3A) to the perturbation matrix derived from the state with combined feedforward and feedback inputs. In the state in which feedforward and feedback drives are combined in the same column, the total number of significant changes (sum of blue and red squares) is smaller than that in the feedforward-driven or feedback-driven state, and less biased towards positive perturbational effects than the feedback-driven state (Supplementary Fig. S1).

Lastly we analyzed the case in which feedforward is constantly present and we put the network in different scenarios varying the feedback input. This resulted in 15 different cases with FB varying from 0 to 80 pA. We conducted a perturbative analysis in each of the states and

quantified the the number of marked changes, further categorizing them into percentages of positive and negative alterations. We replicated these experiments with FB input held constant and varied the strength of FF input instead. In both experimental setups, an increase in the strength of the input consistently led to a decrease in the number of changes in firing rates. Detailed results of these analyses are presented in Supplementary S3.

## Discussion

The intricate dynamics of cortical columns, particularly in response to various excitatory inputs, have long been a subject of interest in neuroscience<sup>1,37</sup>. Our study offers a comprehensive exploration of these dynamics in a data-constrained computational model of a V1 cortical column with a realistic connectivity and multiple cell types and postsynaptic receptors, with an emphasis on dynamic cell-to-cell interactions across four different states: spontaneous, feedforward-driven, feedback-driven, and a feedforward-feedback combination<sup>38,39</sup>.

Our perturbation analysis serves as a valuable predictive tool for experimental tests. We have shown that the response elicited by stimulating a specific neuronal population can vary significantly based on the network's initial state, whether it be spontaneous, driven by feedforward (FF) input, feedback (FB) input, or a combination of FF and FB. This variability in response highlights the critical role of the network's initial conditions in shaping its subsequent dynamics. For example, our model predicts that upon perturbative input to pyramidal cells in layer 2/3, the response of PV cells in layer 5 varies depending on the initial state—being in the spontaneous condition or under feedforward influence. There is a pronounced response in PV cells for the former, while the response becomes negligible for the latter.

Furthermore, we demonstrated the stabilizing effects of feedforward inputs: when the network is in an elicited state, it becomes difficult to perturb. As a result, the change in firing rates due to perturbation inputs will be minimal and often not significant, as shown in Fig. 2D. A similar pattern is observed for states with high feedback inputs, as indicated in Fig. 3C.

Another primary finding of our study is the distinctive roles of inhibitory neurons in network dynamics. For instance, our model predicts that in an experimental setting with strong top-down modulation of V1—such as input to excitatory neurons in layer 5—providing stimuli to different inhibitory neurons in layer 6 will induce contrasting responses in the E2/3 neurons, depending on the specific inhibitory subgroup targeted. This underscores the specialized functions of various inhibitory cell types in a variety of states. Laminar-specific optogenetic stimulation, which has been developed recently<sup>40</sup>, could be used to empirically test these predictions, along with others derived from our model.

Our findings underscore the nuanced, state-dependent interplay between different layers and cell types within the column, in line with previous results on the complex dynamics linked to cell heterogeneity<sup>31,41–44</sup>. The pronounced translaminar inhibition observed when exciting pyramidal neurons in layer 6 (Fig. 4A panel A1), contrasted with the widespread excitation triggered by inputs to pyramidal neurons in layers 2/3 (Fig. 4A panel A4) and 4 (Fig. 1B) shows not only the layered specificity of the cortical processing but also the complicated regulatory mechanism in the neuronal network dynamics. The model suggests that excitation of layer 6 pyramidal cells indeed triggers translaminar inhibition, as previously shown experimentally<sup>28</sup>. However, such overall inhibition is not linked to a simple recruitment of local interneurons in each layer as previously suggested, because different interneuron types (in layer 2/3 and 4) also undergo a decrease in activity. Instead, our model suggests that layer 6-triggered translaminar inhibition is a network effect that involves non-trivial interactions across different layers and cell types.

The mixed effects observed upon stimulating (SST, VIP and PV) interneurons suggests the importance of considering the diverse roles of different neuronal populations within the column<sup>8,45,1,46,5</sup>. For instance, our the perturbation analysis of feedback states (Fig. 4) indicates contrasting effects when perturbing different interneurons types. In contrast to PV cells, perturbations to SST and VIP cells in layer 6 alone never triggered a significant response in pyramidal cells of other layers, with the exception of the last configuration (B4, feedback

targeting pyramidal layer 6). In this particular set up, layer 2/3 pyramidal cells increase their activity when perturbation is applied to layer 6 SST or VIP cells, and decrease it when PV cells were targeted— highlighting cell-type selective modulation across layers. Such a pattern aligns with the classical disinhibitory pathway<sup>41</sup> observed here in a trans-laminarly fashion: elevated SST activity in layer 6 leads to decreased activity in layer 2/3 pyramidal cells. However, this disinhibitory effect was absent in most other states, except in the scenario with feedback to layer 5 (Fig. 3A). This reiterates the critical role of initial network states in interpreting the outcomes of perturbations.

Our model suggests that the dynamics between pyramidal, SST and VIP cells are more complex than what is usually assumed when envisaging a classical disinhibitory pathway<sup>41</sup>. Indeed, SST-mediated disinhibition of pyramidal cells was not observed in our model for most of the states or configurations considered, suggesting that the occurrence of disinhibition in real circuits is likely driven by context-dependent plasticity mechanisms, which aligns with previous experimental and computational results<sup>31,47,48</sup>.

The effects of feedforward and feedback inputs, both individually and in combination, generate different responses . While feedforward inputs generally augmented activity of pyramidal cells across all layers (Fig. 1C), feedback inputs often had an inhibitory effect (Fig. 1D), which became especially evident in layer 6 (Fig. 4-A4). This observation aligns with the notion that feedback mechanisms often serve to modulate lateral inter-columnar interactions (as observed experimentally<sup>33,34</sup>) or fine-tune cortical responses<sup>49</sup>, potentially to optimize information processing or to prevent runaway excitation<sup>50</sup>. Interestingly, the competing effects of feedforward and feedback inputs, when introduced simultaneously, revealed the delicate balance maintained within the columnar circuitry<sup>17,51</sup>. The ability of feedback inputs to L5 to effectively neutralize the impact of feedforward inputs, especially in layer 6, suggests a robust regulatory mechanism at play: inputs to L5 pyramidal cells increase the activity of inhibitory neurons in other layers, such as layer 6, which in turn reduces the activity of pyramidal cells , thereby mitigating the initial increase caused by feedforward inputs. Such dynamics might be

crucial for ensuring that the column operates within an optimal regime, avoiding both hypo- and hyperactivity.

## Limitations

### *Synaptic plasticity*

A further factor which plays an important role in generating rich neuronal dynamics is synaptic plasticity, which we have not incorporated in the model for the purposes of this work.

Processes such as short-term synaptic plasticity and spike-time dependent plasticity have been shown to result in complex behaviors such as neuronal oscillations<sup>28</sup>. Synaptic plasticity and neuronal oscillations are critical for learning, memory, and coordinated neural activity. Further iterations of the model could incorporate these elements to investigate how long-term changes in synaptic efficacy and oscillatory patterns might influence the function and stability of the cortical column within the various conditions analyzed in this work. Moreover, exploring perturbations in such plastic models would provide a deeper understanding of neural dynamics. Nonetheless, the perturbations responses in our current model, even without incorporating synaptic plasticity, hints at how such plasticity might modulate working memory and learning processes. If the column shows increased sensitivity to perturbations under certain conditions, it may suggest a heightened capacity for synaptic changes at the basis of learning and memory formation.

### *Multi-compartmental neurons*

In this work, we employed a leaky integrate-and-fire (LIF) neuron model. Introducing multi-compartmental neurons would add significant biological detail, offering a richer exploration of biophysical network dynamics. A single-compartment model, as used here, restricts our capacity to simulate the intricate intracellular processes occurring within actual neuronal structures. Multi-compartment models could simulate dendritic processing and back-propagating action potentials, offering a more detailed understanding of how individual neurons contribute to overall columnar activity. Such an expansion could enhance our

comprehension of local processing within neurons and how activity propagates through the network. However, a multi-compartment approach adds complexity, potentially overcomplicating the model, making it more challenging to manage. This is why multi-compartments were not included in the current model, as they likely wouldn't significantly affect the results concerning overall perturbation dynamics.

#### *Thalamus and higher order structures*

Our model's structure also lacks the thalamus; thalamic input is approximated as currents targeting layer 4, omitting direct modeling of the thalamus and the V1-LGN feedback loops that are integral to visual processing and attention mechanisms. Nevertheless, the simulation of external inputs to layer 4 neurons in our simulations may mimic the effects of thalamocortical loops. Incorporating thalamic interactions would enhance the model by simulating more accurate sensory input dynamics and enabling the exploration of attentional modulation on cortical column function. Future models could include thalamic inputs to study their effects on cortical computations, which is particularly relevant to conditions like schizophrenia, where thalamocortical interactions are frequently disrupted<sup>52</sup>.

The absence of higher-order structures is another limitation; feedback from higher areas is modeled as currents targeting different layers but a comprehensive study of the interactions with higher visual areas is not included. Additionally, the model does not currently simulate natural stimuli, which could drastically change the responses of the cortical column due to the complexity and variability inherent in real-world inputs. An explicit study of natural stimuli would require mapping visual inputs directly to layer 4 neurons (each pixels as an input current), potentially revealing aspects of sensory encoding and processing in the cortex. However, such an investigation was beyond the scope of this study.

#### **Implications of the model**

A recent study emphasize the unique role of layer 5 (L5) neurons in subcortical loops, which participate in feedback mechanism into the cortex and thalamus<sup>49,1</sup>. Our analysis highlights the importance of L5 in counterbalancing feedforward excitation and shows the significance of this layer in both FF and FB processing. Given the special interest in L5 cells, our model can serve as a predictive tool for the effects of perturbations on this layer and help in designing relevant experiment, thereby affirming the functional significance of this layer. We can speculate that the modulation of activity in L5 cells may have far-reaching implications for the tuning of cortical-thalamic interactions, potentially affecting sensory processing and cognitive functions associated with these pathways.

The perturbation approach utilized in our study could be adopted more broadly as an analytical tool in other computational models, such as those exploring predictive coding in the visual cortex<sup>54</sup>. For example, this approach could benefit models that incorporate interneurons, to dissect the individual and collective contributions of interneurons to network behavior, thus enhancing our understanding of their roles in cortical computations.

Our model reveals cascading effects across various neuronal types, which presents a challenge for decoding specific roles of these cells in predictive coding<sup>55</sup> (PC) frameworks. Identifying which neurons are responsible for coding errors or predictions becomes complex when considering the multitude of interactions in the complex dynamics of our cortical column model.

However, this complexity is reflective of the nature of cortical computations and suggests that understanding coding in such networks may require an approach which looks at emergent properties rather than reductionist approaches. The current model can suggest experiments that may be conducted within simplified, rate-based models. Such models could be better suited for this exploration and to determine which cell types encode errors or predictions.

Lastly, our findings reveal a stabilizing effect of feedforward (FF) input, hinting that cortical columns may be inherently constructed to provide stability and resilience against

perturbations. This resilience could be a natural consequence of the need for reliable information processing in the face of constantly changing environmental inputs. Our observations could inform hypotheses regarding the evolution of neural architectures in the cortex, optimized for maintaining stability while allowing for the flexibility required for adaptive behavior.

#### *Relevance to Cortical Tasks*

Our findings may have implications for tasks involving the cortex, such as working memory and contextual learning. The E/I balance, central to our cortical column model, is crucial for the proper functioning of cortical circuits involved in these cognitive functions. Disruptions in this balance have been linked to cognitive deficits and neuropsychiatric disorders. All interneuron types in the model contribute to maintaining a balanced network, and the state-dependent effects offer insights into how the cortex might adapt to cognitive tasks. For instance, tasks involving working memory often require information manipulation based on the current cognitive context, and our model suggests that cortical responses to such tasks may vary significantly with the underlying state of neural activity. Integrating feedforward and feedback information is crucial for complex cognitive tasks, and our findings on the distinct effects of these input types may relate to how the cortex integrates sensory information with higher-order cognitive processes during contextual learning.

## **Conclusion**

Previous research has highlighted the challenges of predicting activity changes in cortical circuits based on simple intuitions<sup>56</sup>. The multifaceted interactions between different cell types, layers, and input modalities necessitate a detailed computational approach to grasp the underlying mechanisms. In conclusion, our findings provide valuable insights into the operational intricacies of cortical columns, emphasizing the importance of both feedforward and feedback-induced state changes in shaping neural responses.

The role of PV cells and NMDA receptors in modulating E/I balance points to their potential involvement in the pathology of neurological disorders where this balance is disrupted such as schizophrenia and autism. Our results highlight the delicate equilibrium required for proper cognitive functioning, and suggest that disruptions in this balance may contribute to the cognitive and behavioral disturbances characteristic of these conditions. Future studies might delve deeper into the specific molecular and biophysical mechanisms that underlie these dynamics, potentially paving the way for targeted therapeutic interventions in disorders marked by such neural imbalances.

## Methods

The comprehensive architecture of the model and all parameter specifications are detailed in the methods section of Moreni et al.<sup>21</sup>. Below, we provide again the main features.

### Model architecture

The cortical column model, shown in Fig. 1, is composed of a total number ( $N_{\text{total}}$ ) of 5,000 neurons. The model consists of four cortical layers each containing pyramidal neurons, PV, SST and VIP cells (layers 2/3, 4, 5, 6) and one layer containing only VIP cells (layer 1). Each of the four ‘complete’ layers harboured pyramidal neurons (85% of cells) and inhibitory interneurons (15%; each inhibitory group in a given layer was represented by a particular percentage out of this 15%). The fractional sizes of neuron types in each layer (of the total number in the column) and those of each cell type in each layer were taken from the Allen institute database<sup>57</sup> and are reported in Supplementary Tables 1 and 2. All neurons received background noise modelled as coming from the rest of the brain (Fig. 1). The levels of background noise that each type of cell received can be found in Supplementary Table 9, the tuned spontaneous firing rate effectuated by the Poissonian spike generators underlying noise generation connected to each group differed amongst cell types.

We use the term *connection* with reference to subpopulations or groups, defined by the pre- and postsynaptic neuron types and the layer they are in. The connection probability defines the

probability for each possible pair of pre- and postsynaptic neurons to form a connection between them. If  $p=0.1$  this connects all neuron pairs of the two specific groups with a probability of 10%. The connectivity probability matrix  $P$  is defined by the  $16 \times 16 + 16 \times 2 = 288$  connection probabilities  $p$  between the 17 considered cell groups (4 types in each of the 4 layers plus 1 group in layer 1; a group thus potentially receives inputs from the other 16 cell groups and also potentially projects to all of them). The connection probability matrix  $P$  used to constrain the model is available in the portal of the Allen Institute database (<https://portal.brain-map.org/explore/models/mv1-all-layers>). Each connection has also a particular strength which differs per neuron group. Thus, the strength was specified at the level of neuron type X projecting to neuron type Y. The strengths of connections between neurons are constrained using the matrix  $S$  available at <https://portal.brain-map.org/explore/models/mv1-all-layers>. How we set the strengths of single synapse using the matrix  $S$  is explained below (Eq. 11).

We illustrate how any two groups (X and Y) are connected with an example: VIP cells in layer 1 (X) that have a connection going to SST cells in layer 4 (Y) will all have the same connection strength. However, not all VIP cells in layer 1 are connected to SST cells in layer 4 because they connect with probability  $p$ .

### Neuron Model

All pyramidal cells and all three types of interneuron are modelled as leaky integrate-and-fire neurons. Each type of cell is characterized by its own, individual set of parameters: a resting potential  $V_{rest}$ , a firing threshold  $V_{th}$ , a membrane capacitance  $C_m$ , a membrane leak conductance  $g_L$  and a refractory period  $\tau_{ref}$ . The corresponding membrane time constant is  $\tau_m = C_m/g_L$ . The membrane potential  $V(t)$  of a cell is given by:

$$C_m \frac{dV(t)}{dt} = -g_L(V(t) - V_{rest}) + I_{syn}(t) \quad (\text{Eq. 1})$$

where  $I_{syn}(t)$  represents the total synaptic current flowing into the cell.

At each time point of the simulation, a neuron integrates the total incoming current  $I_{syn}(t)$  to update its membrane potential  $V(t)$ . When the threshold  $V_{th}$  is reached a spike is generated, followed by an instantaneous reset of the membrane potential to the resting membrane potential  $V_{rest}$ . Then, for a refractory period  $\tau_{ref}$ , the membrane potential stays at its resting value  $V_{rest}$  and no spikes can be generated. After  $\tau_{ref}$  has passed, the membrane potential can be updated again (see Tables S4-S8 for corresponding parameter values).

### Model of synapses

Each cell group in each layer is connected to all the other groups of the cortical column with its own synaptic strength and probability. The values in matrix  $P$  indicate the probability that a neuron in group A (e.g. the PV cells in layer 4) is connected to a neuron in group B (e.g. the SST cells in layer 5). Excitatory postsynaptic currents (EPSCs) have two components mediated by AMPA and NMDA receptors, respectively. Inhibitory postsynaptic currents (IPSCs) are mediated by GABA<sub>A</sub> receptors.

The inputs to model neurons consist of three main components: background noise, external (e.g. sensory) input and recurrent input from within the column. EPSCs due to background noise are mediated in the model exclusively by AMPA receptors ( $I_{bg,AMPA}(t)$ ) and EPSCs due to external stimuli (i.e. originating from outside the column) are represented by  $I_{ext}(t)$ . The recurrent input from within the column is given by the sum of  $I_{AMPA}(t)$ ,  $I_{NMDA}(t)$ ,  $I_{GABA}(t)$ . These are all the inputs from all the other (presynaptic) neurons projecting to the neuron under consideration.

The total synaptic current that each neuron receives is given by:

$$I_{syn}(t) = I_{ext}(t) + I_{bg,AMPA}(t) + I_{AMPA}(t) + I_{NMDA}(t) + I_{GABA}(t) \quad (\text{Eq. 2})$$

with the last four terms given by

$$I_{bg,AMPA}(t) = g_{AMPA}(V(t) - V_E)s_{bg,AMPA}(t) \quad (\text{Eq. 3})$$

$$I_{AMPA}(t) = g_{AMPA}(V(t) - V_E)\sum_{j=1}^N w_j s_j^{AMPA}(t) \quad (\text{Eq. 4})$$

$$I_{GABA}(t) = g_{GABA}(V(t) - V_I)\sum_{j=1}^N w_j s_j^{GABA}(t) \quad (\text{Eq. 5})$$

$$I_{NMDA}(t) = \frac{g_{NMDA}(V(t) - V_E)}{1 + [\text{Mg}^{2+}] \exp(-\frac{0.062V(t)}{3.57})} \sum_{j=1}^N w_j s_j^{NMDA}(t) \quad (\text{Eq. 6})$$

where the reversal potentials are  $V_E=0$  mV,  $V_I = V_{rest}$ , and each group of inhibitory interneurons has its own  $V_{rest}$ . The  $g$  terms represent the conductances of the specific receptor types. The weights  $w_j$  represent the strength of each synapse received by the neuron. The sum runs over all presynaptic neurons  $j$  projecting to the neuron under consideration. NMDAR currents have a voltage dependence controlled by extracellular magnesium concentration<sup>58</sup>,  $[\text{Mg}^{2+}]=1$  mM. The  $s$  terms represent the gating variables, or fraction of open channels and their behaviour is governed by the following equations.

First, the AMPAR channels are described by

$$\frac{ds_j^{AMPA}(t)}{dt} = \frac{-s_j^{AMPA}(t)}{\tau_{AMPA}} + \sum_k \delta(t - t_j^k) \quad (\text{Eq. 7})$$

where the decay time constant of the AMPA currents is  $\tau_{AMPA}=2$  ms, and the sum over  $k$  represents the contribution of all spikes (each of which is indicated by delta,  $\delta$ ) emitted by presynaptic neuron  $j$ . In the case of background AMPA currents (Eq. 3), the spikes are emitted according to a Poisson process with rate  $v_{bg}$ . Each group of cells in each layer is receiving a different Poisson rate of background noise (see Table S9).  $v_{bg}$  is cell-specific, hence each has a specific firing pattern.

The gating of single NMDAR channels is described by

$$\frac{ds_j^{NMDA}(t)}{dt} = \frac{-s_j^{NMDA}(t)}{\tau_{NMDA,decay}} + \alpha x_j(t)(1 - s_j^{NMDA}(t)) \quad (\text{Eq. 8})$$

$$\frac{dx_j(t)}{dt} = \frac{-x_j(t)}{\tau_{NMDA,rise}} + \sum_k \delta(t - t_j^k) \quad (\text{Eq. 9})$$

where the decay and rise time constants of NMDAR current are 80 ms and 2 ms respectively, and the constant  $\alpha=0.5 \text{ ms}^{-1}$ . The GABA<sub>A</sub> receptor synaptic variable is described by

$$\frac{ds_j^{GABA}(t)}{dt} = \frac{-s_j^{GABA}(t)}{\tau_{GABA}} + \sum_k \delta(t - t_j^k) \quad (\text{Eq. 10})$$

where the decay time constant of GABA<sub>A</sub> receptor current is 5 ms.

#### Parameters of the model:

As previously mentioned, each type of cell in each layer is characterized by its own set of parameters: a resting potential  $V_{rest}$ , a firing threshold  $V_{th}$ , a membrane capacitance  $C_m$ , a membrane leak conductance  $g_L$  and a refractory period  $\tau_{ref}$ . The parameter setting s were taken from the Allen Institute database (<https://portal.brain-map.org/explore/models/mv1-all-layers>). In particular, for each type of cell in each layer the Allen database proposes different subsets of cells (e.g. two different PV subsets in L4), each with his own set of parameters. To simplify the model, we only used one set of parameters for each cell type in each layer, choosing the set of parameters of the most prevalent subset of cells. The parameters  $C_m$ ,  $g_L$ ,  $\tau_{ref}$ ,  $V_{rest}$ ,  $V_{th}$  used for each cell type in each layer are reported in Tables S4-S8.

#### Details on background noise:

All neurons received background noise, representing the influence of the 'rest of the brain' on the modeled area, as shown in Figure 1. Excitatory postsynaptic currents (EPSCs) due to

background noise are exclusively mediated in the model by AMPA receptors, denoted as  $I_{bg,AMPA}(t)$  (Eq. 3). The levels of background noise that each group of cells received can be found in Supplementary Table 9. The firing rate  $v_{bg}$  of the background Poissonian pulse generators connected to each group differed among each cell type. Each neuron in every group was connected to its own background Poisson generator. Thus, even though the rates  $v_{bg}$  of the Poisson generators were the same for all neurons within the same group, each specific cell received its own specific pulse train.

#### Details on synaptic weights:

The weight of each synapse  $w_j$  from neurons of group A to neurons in group B was set as follows:

$$w_j = G * \frac{\hat{s}}{N_{send} p} \quad (\text{Eq. 11})$$

where  $G=5$  is the global coupling factor,  $\hat{s}$  is the overall strength between the two connected groups of cells,  $N_{send}$  is the number of neurons in the sending population A, and  $p$  the probability of connection between the neurons of the two groups (A and B) taken from the experimental probability matrix  $P$ . For each pair of connected groups,  $\hat{s}$  is taken from the experimental synaptic connectivity matrix  $S$ , defined by the  $16 \times 16 + 16 \times 2 = 288$  synaptic strengths between the 17 considered cell types (4 groups in each of the 4 layers + 1 group in layer 1). Matrices  $S$  and  $P$  can be found at <https://portal.brain-map.org/explore/models/mv1-all-layers>. The normalization in Eq. 11 above guarantees that the dynamics and equilibrium points of the system scale properly with the size of the network (Fig. S2).

The spikes generated by a presynaptic excitatory neuron can target AMPA or/and NMDA receptors of the postsynaptic neuron. The AMPA and NMDA receptors are chosen to be present at the excitatory synapse in a 0.8 and 0.2 ratio respectively. Thus, the probability of connection  $p$  between the neurons of the two groups (A and B) is multiplied by 0.2 for NMDA receptors and 0.8 for AMPA receptors. For example, suppose that excitatory neurons in group A are

connected to neurons in group B with a probability  $p$  (taken from the matrix P). Then the excitatory connections targeting the AMPA receptors of group B will be chosen with  $p_{AMPA} = p * 0.8$  and those targeting NMDA receptors will be chosen with  $p_{NMDA} = p * 0.2$ .

All differential equations were numerically solved using Euler's method, using a time step of 0.1 ms.

### Perturbation matrix

We analysed the effects on neuronal populations following the administration of a specific input. Each square in a matrix (e.g. figure 2A) corresponds to an individual simulation. The y-axis specifies the population receiving the input, while the x-axis indicates the observed effect on a different population. To create the matrices, we injected a 30 pA constant current into each group and recorded the ensuing effects on all other neuronal groups. The percentage change in average firing rate, used to construct these matrices, was determined by comparing the mean firing rates after stimulation with the respective baseline rates (prior to input injection). To evaluate the baseline rates we used a time window of 3 seconds of simulation, the same time window was used to evaluate the rates after the injected current. We thus calculated the mean firing rate for each population both before and after the stimuli were introduced. In the matrices, red signifies an increase in firing rate by 20% or more relative to the baseline, blue indicates a decrease in firing rate by 20% or more, and white reflects a change in firing rate that is less than 20% (whether a decrease or an increase).

It is important to understand that these 'baselines' for firing rates (initial states) varied depending on the scenario under analysis: Spontaneous, FF input (with different strength), FB input, or a combination of the two. We always compared the firing rates after the perturbation stimuli with the firing rates prior the input injection, which was specific for each initial state analysed.

### Random seed

When performing the simulations, we made sure to use the same random seed for each run. This way, all the random variables in the network (noise, the exact number of connections between neurons) were always kept constant. This method allows us to ensure that the changes in the cells' firing rates from one simulation to the other were due to the perturbation under examination and not to other fluctuations or variables.

### Comparison Matrix

The comparison matrix displayed in Fig. 2C was constructed as follows: a white square indicates no change in the firing rate of a specific population when comparing the spontaneous case to e.g. the FF case. This can occur when the two perturbation matrices we are comparing had both a red squares, both a blue squares or both a white squares (Fig. 2A- 2B).

A red square represents one of the following scenarios:

- A transition from a non-significant alteration (<20% or <-20% in absolute terms) to a significant increase (>20%).
- A transition from a significant decrease (> -20% in absolute terms) to a non-significant alteration (<20% or <-20% in absolute terms).
- A transition from a significant decrease (> -20%) to a significant increase (>20%).

A green square indicates one of the following conditions:

- A transition from a significant increase (>20%) to a significant decrease (> -20% in absolute terms).
- A transition from a significant increase (>20%) to a non-significant alteration.
- A transition from a non-significant alteration to a significant decrease (> -20%).

**Acknowledgments:**

This work was done with the support of EBRAINS and HBP computing services. We thank Matthias Brucklacher, Kwangjun Lee and Parva Alavian for constructive discussions, and Hans Ekkehard Plessner, Sacha van Albada, Walter Senn and Sander Bohte for their useful feedback on early iterations of the work.

**Funding:** This project has received funding from the European Union's Horizon 2020 Framework Programme for Research and Innovation under the Specific Grant Agreement No. 945539 (Human Brain Project SGA3; to CMAP, JFM), the NWA-ORC grant NWA.1292.19.298 (JFM, CMAP), a UvA/ABC Project Grant (JFM) and NWO-ENW-M2 grant OCENW.M20.285 (CMAP).

**Author contributions:** JFM, GM, CP conceived and designed the study; GM performed the research; GM and JFM analyzed the results; GM, CP and JFM wrote the manuscript.

**Competing interests:** Authors declare no competing interests.

**Data and materials availability:** All information needed to reproduce the results of this manuscript are in the main text and Materials and Methods section, and the code used will be made available upon publication of this work on [GitHub](#).

**References**

1. Douglas, R. J. & Martin, K. A. C. Neuronal circuits of the neocortex. *Annu. Rev. Neurosci.* **27**, 419–451 (2004).
2. McAfee, S. S., Liu, Y., Sillitoe, R. V. & Heck, D. H. Cerebellar Coordination of Neuronal Communication in Cerebral Cortex. *Front. Syst. Neurosci.* **15**, (2022).

3. Mountcastle, V. B. The columnar organization of the neocortex. *Brain J. Neurol.* **120** ( Pt 4), 701–722 (1997).
4. Huang, C., Zeldenrust, F. & Celikel, T. Cortical Representation of Touch in Silico. *Neuroinformatics* **20**, 1013–1039 (2022).
5. Jiang, H.-J., Qi, G., Duarte, R., Feldmeyer, D. & Albada, S. J. van. A Layered Microcircuit Model of Somatosensory Cortex with Three Interneuron Types and Cell-Type-Specific Short-Term Plasticity. 2023.10.26.563698 Preprint at <https://doi.org/10.1101/2023.10.26.563698> (2023).
6. Maex, R. & Gutkin, B. Temporal integration and 1/f power scaling in a circuit model of cerebellar interneurons. *J. Neurophysiol.* **118**, 471–485 (2017).
7. Schwalger, T., Deger, M. & Gerstner, W. Towards a theory of cortical columns: From spiking neurons to interacting neural populations of finite size. *PLOS Comput. Biol.* **13**, e1005507 (2017).
8. Isaacson, J. S. & Scanziani, M. How inhibition shapes cortical activity. *Neuron* **72**, 231–243 (2011).
9. Zhou, S. & Yu, Y. Synaptic E-I Balance Underlies Efficient Neural Coding. *Front. Neurosci.* **12**, (2018).
10. Wilson, H. R. & Cowan, J. D. Excitatory and Inhibitory Interactions in Localized Populations of Model Neurons. *Biophys J* **12**, 1–24 (1972).
11. Yang, W. & Sun, Q.-Q. Circuit-specific and neuronal subcellular-wide E-I balance in cortical pyramidal cells. *Sci. Rep.* **8**, 3971 (2018).
12. Vreeswijk, C. van & Sompolinsky, H. Chaos in Neuronal Networks with Balanced Excitatory and Inhibitory Activity. *Science* **274**, 1724–1726 (1996).

13. Litwin-Kumar, A. & Doiron, B. Slow dynamics and high variability in balanced cortical networks with clustered connections. *Nat. Neurosci.* **15**, 1498–1505 (2012).
14. Ferguson, B. R. & Gao, W.-J. PV Interneurons: Critical Regulators of E/I Balance for Prefrontal Cortex-Dependent Behavior and Psychiatric Disorders. *Front. Neural Circuits* **12**, (2018).
15. Selten, M., van Bokhoven, H. & Nadif Kasri, N. Inhibitory control of the excitatory/inhibitory balance in psychiatric disorders. *F1000Research* **7**, 23 (2018).
16. Bastos, A. M. Visual Areas Exert Feedforward and Feedback Influences through Distinct Frequency Channels. *Neuron* **85**, 390–401 (2015).
17. Mejias, J. F., Murray, J. D., Kennedy, H. & Wang, X.-J. Feedforward and feedback frequency-dependent interactions in a large-scale laminar network of the primate cortex. *Sci. Adv.* **2**, e1601335 (2016).
18. Brosch, T. & Neumann, H. Interaction of feedforward and feedback streams in visual cortex in a firing-rate model of columnar computations. *Neural Netw.* **54**, 11–16 (2014).
19. Markov, N. T. *et al.* Anatomy of hierarchy: Feedforward and feedback pathways in macaque visual cortex. *J. Comp. Neurol.* **522**, 225–259 (2014).
20. Spaak, E., Bonnefond, M., Maier, A., Leopold, D. A. & Jensen, O. Layer-specific entrainment of γ-band neural activity by the α rhythm in monkey visual cortex. *Curr. Biol. CB* **22**, 2313–2318 (2012).
21. Moreni, G., Pennartz, C. M. A. & Mejias, J. F. Synaptic plasticity is required for oscillations in a V1 cortical column model with multiple interneuron types.

22. Binzegger, T., Douglas, R. J. & Martin, K. A. C. A Quantitative Map of the Circuit of Cat Primary Visual Cortex. *J. Neurosci.* **24**, 8441–8453 (2004).
23. Billeh, Y. N. *et al.* Systematic Integration of Structural and Functional Data into Multi-scale Models of Mouse Primary Visual Cortex. *Neuron* **106**, 388-403.e18 (2020).
24. Bastos, A. M., Lundqvist, M., Waite, A. S., Kopell, N. & Miller, E. K. Layer and rhythm specificity for predictive routing. *Proc. Natl. Acad. Sci.* **117**, 31459–31469 (2020).
25. Mejias, J. F. & Wang, X.-J. Mechanisms of distributed working memory in a large-scale network of macaque neocortex. *eLife* **11**, e72136 (2022).
26. Feng, M., Bandyopadhyay, A. & Mejias, J. F. Emergence of distributed working memory in a human brain network model. 2023.01.26.525779 Preprint at <https://doi.org/10.1101/2023.01.26.525779> (2023).
27. Olsen, S. R., Bortone, D. S., Adesnik, H. & Scanziani, M. Gain control by layer six in cortical circuits of vision. *Nature* **483**, 47–52 (2012).
28. Bortone, D. S., Olsen, S. R. & Scanziani, M. Translaminar Inhibitory Cells Recruited by Layer 6 Corticothalamic Neurons Suppress Visual Cortex. *Neuron* **82**, 474–485 (2014).
29. Kok, P., Bains, L. J., van Mourik, T., Norris, D. G. & de Lange, F. P. Selective Activation of the Deep Layers of the Human Primary Visual Cortex by Top-Down Feedback. *Curr. Biol.* **26**, 371–376 (2016).
30. Harris, J. A. *et al.* Hierarchical organization of cortical and thalamic connectivity. *Nature* **575**, 195–202 (2019).

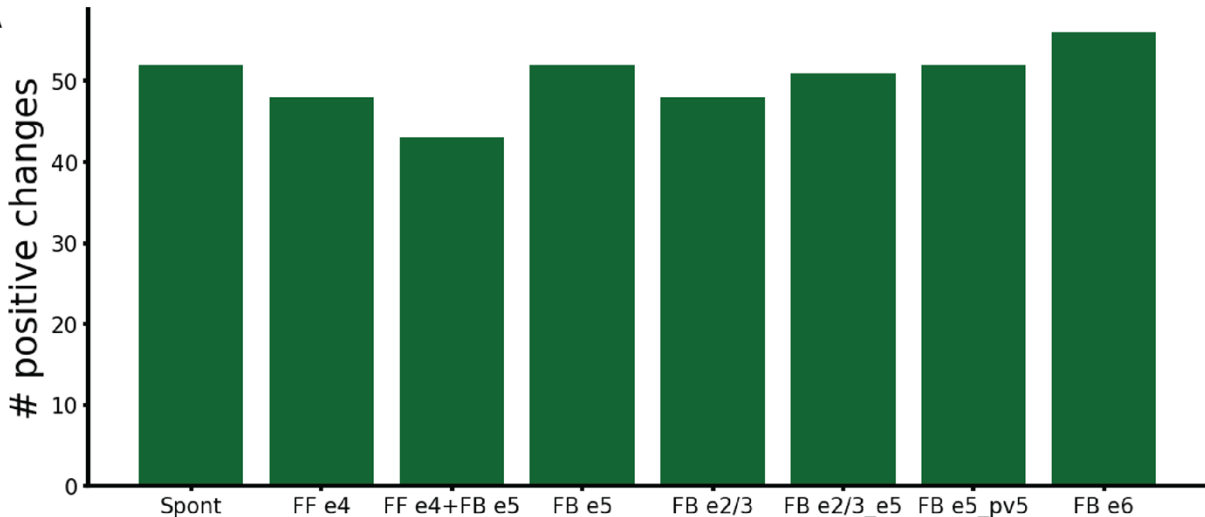
31. Garcia del Molino, L. C., Yang, G. R., Mejias, J. F. & Wang, X.-J. Paradoxical response reversal of top-down modulation in cortical circuits with three interneuron types. *eLife* **6**, e29742 (2017).
32. Miller, E. K., Lundqvist, M. & Bastos, A. M. Working Memory 2.0. *Neuron* **100**, 463–475 (2018).
33. Ramalingam, N., McManus, J. N. J., Li, W. & Gilbert, C. D. Top-Down Modulation of Lateral Interactions in Visual Cortex. *J. Neurosci.* **33**, 1773–1789 (2013).
34. Freeman, E., Driver, J., Sagi, D. & Zhaoping, L. Top-Down Modulation of Lateral Interactions in Early Vision: Does Attention Affect Integration of the Whole or Just Perception of the Parts? *Curr. Biol.* **13**, 985–989 (2003).
35. Rockland, K. S. Notes on Visual Cortical Feedback and Feedforward Connections. *Front. Syst. Neurosci.* **16**, 784310 (2022).
36. Felleman, D. J. & Van Essen, D. C. Distributed hierarchical processing in the primate cerebral cortex. *Cereb. Cortex N. Y. N* **1991** **1**, 1–47 (1991).
37. Schuman, B. & Rudy, B. Dynamics of Neuronal Activity in the Cortical Column during Behavior: Both Neuron Type and Layers Matter. *Neuron* **104**, 186–188 (2019).
38. Callaway, E. M. Feedforward, feedback and inhibitory connections in primate visual cortex. *Neural Netw.* **17**, 625–632 (2004).
39. Lamme, V. A., Supèr, H. & Spekreijse, H. Feedforward, horizontal, and feedback processing in the visual cortex. *Curr. Opin. Neurobiol.* **8**, 529–535 (1998).
40. Suzuki, M., Aru, J. & Larkum, M. E. Double- $\mu$ Periscope, a tool for multilayer optical recordings, optogenetic stimulations or both. *eLife* **10**, e72894 (2021).

41. Lee, S., Kruglikov, I., Huang, Z. J., Fishell, G. & Rudy, B. A disinhibitory circuit mediates motor integration in the somatosensory cortex. *Nat. Neurosci.* **16**, 1662–1670 (2013).
42. Mejias, J. F. & Longtin, A. Optimal Heterogeneity for Coding in Spiking Neural Networks. *Phys. Rev. Lett.* **108**, 228102 (2012).
43. Mejias, J. F. & Longtin, A. Differential effects of excitatory and inhibitory heterogeneity on the gain and asynchronous state of sparse cortical networks. *Front. Comput. Neurosci.* **8**, (2014).
44. Litwin-Kumar, A., Rosenbaum, R. & Doiron, B. Inhibitory stabilization and visual coding in cortical circuits with multiple interneuron subtypes. *J. Neurophysiol.* **115**, 1399–1409 (2016).
45. Buia, C. I. & Tiesinga, P. H. Role of Interneuron Diversity in the Cortical Microcircuit for Attention. *J. Neurophysiol.* **99**, 2158–2182 (2008).
46. Myers-Joseph, D., Wilmes, K. A., Fernandez-Otero, M., Clopath, C. & Khan, A. G. Disinhibition by VIP interneurons is orthogonal to cross-modal attentional modulation in primary visual cortex. *Neuron* **112**, 628-645.e7 (2024).
47. Pakan, J. M. *et al.* Behavioral-state modulation of inhibition is context-dependent and cell type specific in mouse visual cortex. *eLife* **5**, e14985 (2016).
48. Dipoppa, M. *et al.* Vision and Locomotion Shape the Interactions between Neuron Types in Mouse Visual Cortex. *Neuron* **98**, 602-615.e8 (2018).
49. oude Lohuis, M., Cerván, A., Pennartz, C. & Olcese, U. Higher Order Visual Areas Enhance Stimulus Responsiveness in Mouse Primary Visual Cortex. *Cereb. Cortex* **32**, (2021).
50. Tiesinga, P. & Sejnowski, T. J. Cortical Enlightenment: Are Attentional Gamma Oscillations Driven by ING or PING? *Neuron* **63**, 727–732 (2009).

51. Renart, A. The Asynchronous State in Cortical Circuits. *Science* **327**, 587–590 (2010).
52. Zhang, Y. *et al.* Disrupted thalamo-cortical connectivity in schizophrenia: A morphometric correlation analysis. *Schizophr. Res.* **153**, 129–135 (2014).
53. Suzuki, M., Pennartz, C. M. A. & Aru, J. How deep is the brain? The shallow brain hypothesis. *Nat. Rev. Neurosci.* **24**, 778–791 (2023).
54. Lee, K., Dora, S., Mejias, J. F., Bohte, S. M. & Pennartz, C. M. A. Predictive coding with spiking neurons and feedforward gist signalling. *Front. Comput. Neurosci.* **18**, (2024).
55. Rao, R. P. N. & Ballard, D. H. Predictive coding in the visual cortex: a functional interpretation of some extra-classical receptive-field effects. *Nat. Neurosci.* **2**, 79–87 (1999).
56. Yizhar, O. *et al.* Neocortical excitation/inhibition balance in information processing and social dysfunction. *Nature* **477**, 171–178 (2011).
57. Billeh, Y. N. *et al.* Systematic Integration of Structural and Functional Data into Multi-scale Models of Mouse Primary Visual Cortex. *Neuron* **106**, 388-403.e18 (2020).
58. Wang, X.-J. Synaptic Basis of Cortical Persistent Activity: the Importance of NMDA Receptors to Working Memory. *J. Neurosci.* **19**, 9587–9603 (1999).

**Supplementary figures:**

**A**



**B**



Figure S1: Number of significant changes (A) and percentages (B) for positive changes in firing rates elicited by all possible perturbations in the spontaneous state(Spont), feedforward-driven state (FF e4), feedforward-feedback combination (FF e4 + FB e5), and feedback-driven state in all its five possible configurations (i.e. targeting pyramidal layer 5 (FB e5), pyramidal layer 2/3 (FB e2/3), pyramidal layer 2/3 and 5 (FB e2/3\_e5), pyramidal and PV layer 5 (FB e2/3\_pv5), and pyramidal layer 6(FB e6)). The complementary numbers for the bottom panel also provide the data for the negative changes. This figure provides extra analysis on the data presented in Fig. 2A, 2B, 3A, 4B, 5C.

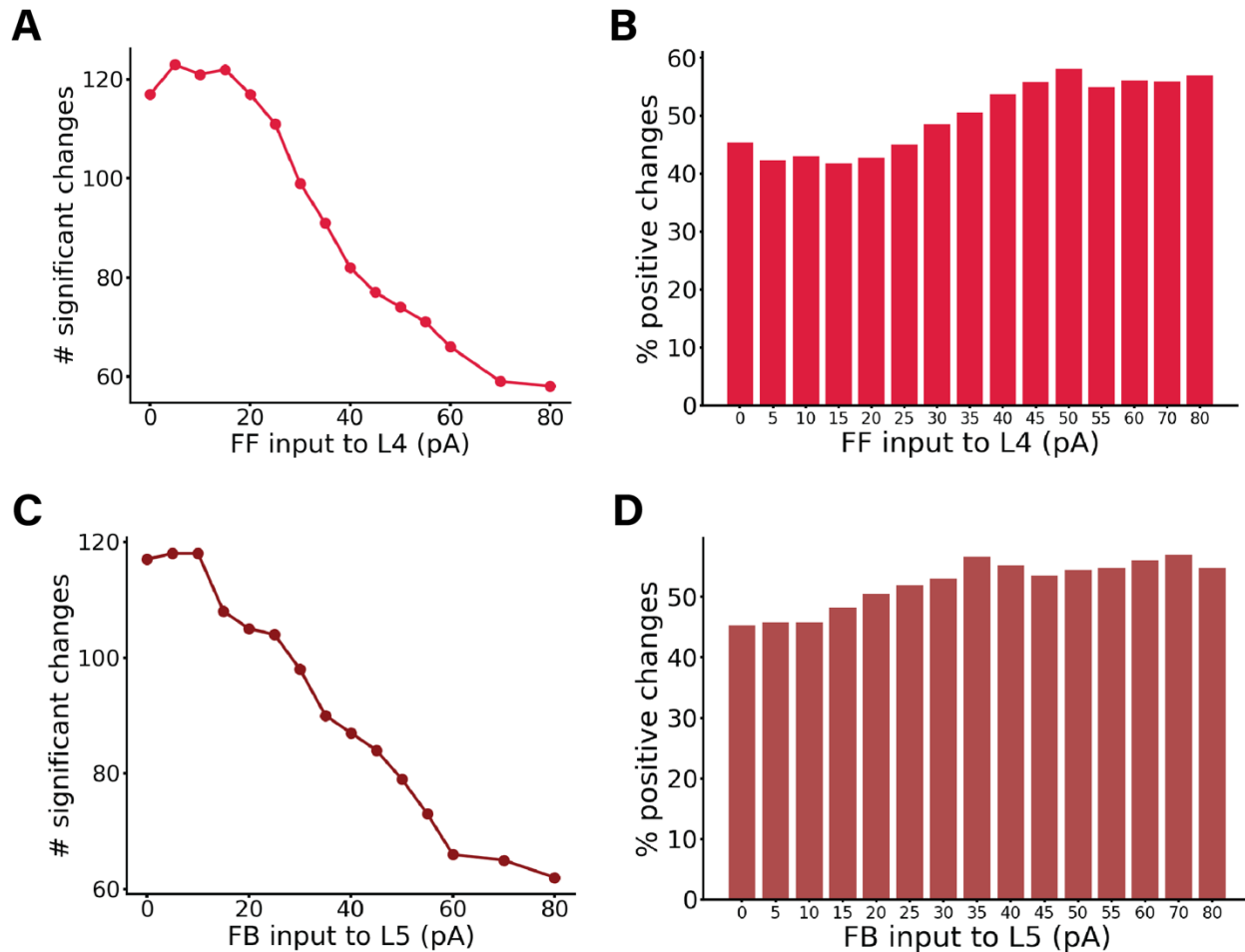


Figure S2: Panels (B) and (D) provide additional information on the data presented in Fig. 2D and Fig. 3C, respectively (shown again here as (A) and (C)).

(A) displays the number of significant changes in the corresponding perturbation matrix. We conducted perturbation analyses for 15 different network conditions, defined by varying feedforward (FF) input to layer 4, resulting in a 16x16 matrix for each cell group, although these matrices are not displayed here. Each condition varied the input strength to excitatory neurons in layer 4, with values on the X-axis ranging from 0 to 80 pA. The Y-axis represents the number of significant alterations in the respective matrix (the sum of red and blue squares). Increased input to layer 4 results in fewer perturbation-induced changes in the firing rates of other populations.

(B) shows percentages of positive changes in firing rates elicited by all possible perturbations in each network state, computed from the total number of significant changes presented in A. The complementary percentages in the panel also provide data for the negative changes.

(C) displays the number of significant changes in the corresponding perturbation matrix for 15 different network conditions, defined by varying feedback (FB) input to layer 5, resulting in a 16x16 matrix for each cell group, although these matrices are not displayed here. Each condition varied the input strength to excitatory neurons in layer 5, with values on the X-axis ranging from 0 to 80 pA. The Y-axis represents the number of significant alterations in the respective matrix (the sum of red and blue squares). Increased input to layer 5 results in fewer perturbation-induced changes in the firing rates of other populations.

(D) presents percentages of positive changes in firing rates elicited by all possible perturbations in each network state, computed from the total number of significant changes shown in C. The complementary percentages in the panel also provide data for the negative changes.

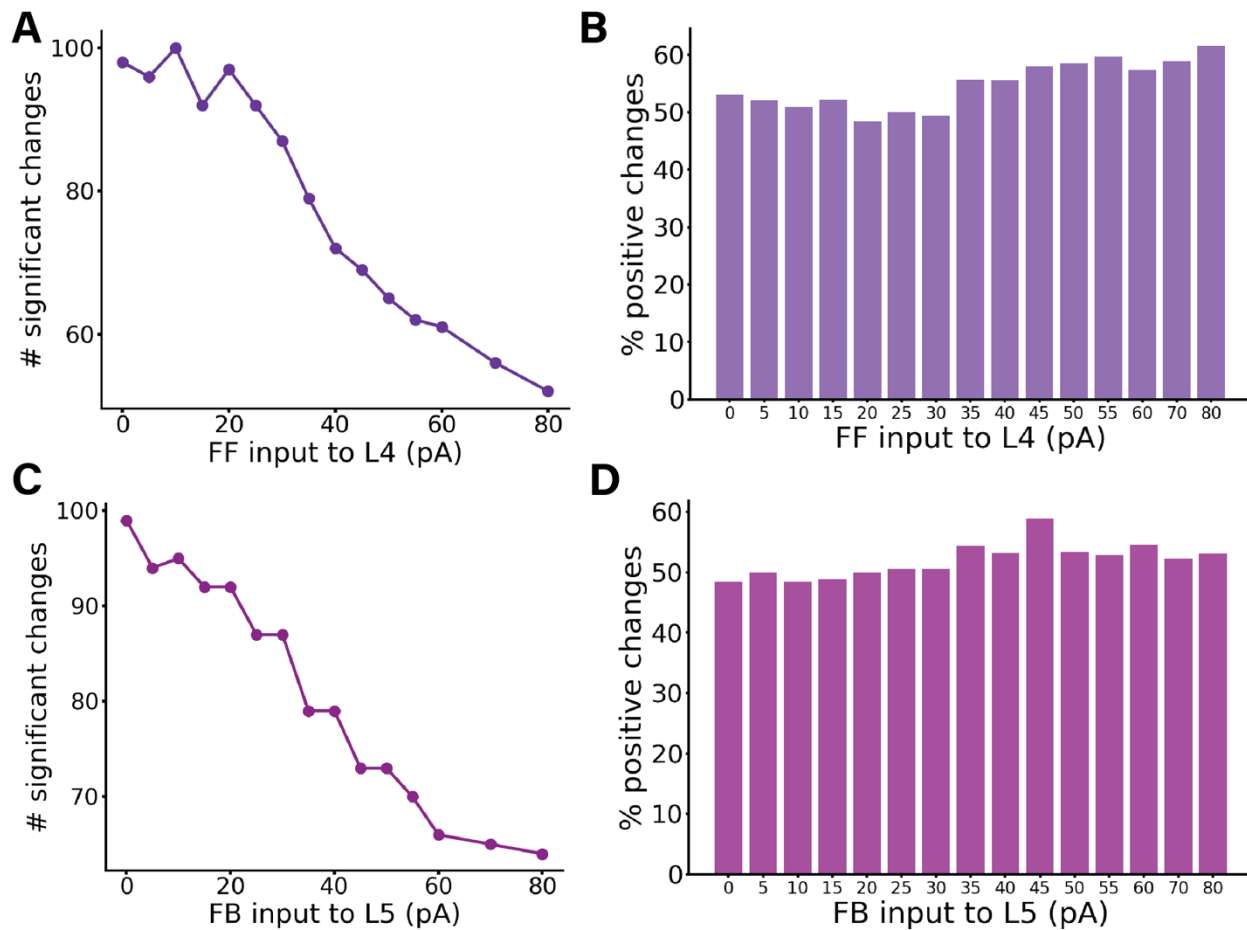


Figure S3: Perturbation Analysis in Different Conditions: A-B) Varying FF input while keeping FB constant. C-D) Varying FB input while keeping FF constant.

(A) displays the number of significant changes in the corresponding perturbation matrix. Perturbation analysis was conducted for 15 different network conditions, defined by varying feedforward (FF) input to layer 4 while keeping feedback (FB) input to pyramidal cells in layer 5 constant at 30 pA, resulting in a 16x16 matrix for each cell group, although these matrices are not displayed here. Each condition varied the input strength to excitatory neurons in layer 4, with values on the X-axis ranging from 0 to 80 pA. The Y-axis represents the number of significant alterations in the respective matrix (the sum of red and blue squares). Increased input to layer 4 results in fewer perturbation-induced changes in the firing rates of other populations.

(B) presents percentages of positive changes in firing rates elicited by all possible perturbations in each network state, computed from the total number of significant changes shown in A. The complementary percentages in the panel also provide data for the negative changes.

(C) illustrates the number of significant changes in the corresponding perturbation matrix. Perturbation analysis was conducted for 15 different network conditions, defined by varying feedback (FB) input to layer 5, and resulting in a 16x16 matrix for each cell group, though these matrices are not displayed here. Each condition varied the input strength to excitatory neurons in layer 5, with values on the X-axis ranging from 0 to 80 pA. The Y-axis represents the number of significant alterations in the respective matrix (the sum of red and blue squares). Increased input to layer 5 results in fewer perturbation-induced changes in the firing rates of other populations.

(D) shows percentages of positive changes in firing rates elicited by all possible perturbations in each network state. The percentage is computed from the total number of significant changes presented in C. The complementary percentages for the panel also provide data for the negative changes.

## **Supplementary Tables:**

### **Tables**

*Table 1: Number of neurons in each layer.  $N_{tot}$  is the total number of cells in the column and can be defined arbitrarily for a simulation. The number of cells in each layer will scale accordingly<sup>23</sup>. We used  $N_{tot}=5000$  for simulations.*

Number of neurons	
L1	0.0192574218*N <sub>tot</sub>
L2/3	0.291088453*N <sub>tot</sub>
L4	0.237625904*N <sub>tot</sub>
L5	0.17425693*N <sub>tot</sub>
L6	0.297031276*N <sub>tot</sub>

*Table 2: Percentage of inhibitory cell types as a fraction of the total number of inhibitory cells in each layer. In each layer, the inhibitory cells represent 15% of the total number of neurons for that layer<sup>23</sup>.*

Percentage (%)	PV	SST	VIP
L2/3	0.295918	0.214286	0.489796
L4	0.552381	0.295238	0.152381
L5	0.485714	0.428571	0.085714
L6	0.458333	0.458333	0.083333

*Table 3: Cell counts in the network for  $N_{tot} = 5000$ .*

Number of neurons	E	PV	SST	VIP
L1				96
L2/3	1236	65	47	107
L4	1010	98	53	27
L5	741	63	56	11
L6	1263	102	102	19

*Table 4: Membrane capacitance for each group of cells. The values are taken from the Allen database<sup>22</sup>. The same values are used for all simulations.*

C <sub>m</sub> (pF)	E	PV	SST	VIP

L1				37.11
L2/3	123.41	70.95	82.34	41.23
L4	80.16	81.21	132.86	40.3
L5	149.43	70.9	52.32	59.29
L6	99.96	49.65	96.09	65.87

Table 5: Leak conductance for each group of cells<sup>23</sup>.

$g_L$ (nS)	E	PV	SST	VIP
L1				4.07
L2/3	2.47	9.49	3.17	6.4
L4	5.16	9.19	7.96	1.87
L5	16.66	5.21	3.43	6.52
L6	5.88	6.86	2.99	6.09

Table 6: Refractory period for each group of cells<sup>23</sup>.

$\tau_{ref}$ (ms)	E	PV	SST	VIP
L1				3.5
L2/3	3	1.26	1.85	2.75
L4	4.4	1.5	2.2	2.4
L5	4.25	1.85	1.9	2.55
L6	3.3	1.65	2.1	2.85

Table 7: Resting membrane potential for each group of cells<sup>23</sup>.

$V_{rest}$ (mV)	E	PV	SST	VIP
L1				-65.5
L2/3	-80.97	-82.35	-69.16	-67.94
L4	-72.53	-70.45	-74.2	-63.14
L5	-68.28	-77.5	-70.01	-72.00
L6	-77.5	-76.42	-62.99	-78.85

*Table 8: Spike threshold for each group of cells<sup>23</sup>.*

$V_{th}$ (mV)	E	PV	SST	VIP
L1				-40.20
L2/3	-40.53	-56.32	-39.95	-41.34
L4	-47.63	-44.23	-44.07	-40.89
L5	-40.55	-51.2	-47.38	-51.2
L6	-42.31	-49.06	-37.19	-44.81

*Table 9: Background noise rate that each group receives. Values represent the Poisson generator rates  $v_{bg}$ .*

Rate of Poisson generator $v_{bg}$ (Hz)	E	PV	SST	VIP
L1				650
L2/3	736	2949	631	1079
L4	1077	1894	2006	152
L5	3460	1399	648	1394
L6	1525	1540	590	1609